

Two-dimensional magnetotelluric inversion of blocky geoelectrical structures

S. Mehanee and M. Zhdanov

Department of Geology and Geophysics, University of Utah, Salt Lake City, Utah, USA

Received 30 November 1999; revised 16 October 2000; accepted 22 August 2001; published 13 April 2002.

[1] This paper demonstrates that there are alternative approaches to the magnetotelluric (MT) inverse problem solution based on different types of geoelectrical models. The traditional approach uses smooth models to describe the conductivity distribution in underground formations. In this paper, we present a new approach, based on approximating the geology by models with blocky conductivity structures. We can select one or another class of inverse models by choosing between different stabilizing functionals in the regularization method. The final decision, whose approach may be used for the specific MT data set, is made on the basis of available geological information. This paper describes a new way of stabilizing two-dimensional MT inversion using a minimum support functional and shows the improvement that it provides over traditional methods for geoelectrical models with blocky structures. The new method is applied to MT data collected for crustal imaging in the Carrizo Plain in California and to MT data collected for mining exploration by INCO Exploration. *INDEX TERMS:* 0644 Electromagnetics: Numerical methods; 3260 Mathematical Geophysics: Inverse theory; *KEYWORDS:* Electromagnetic, magnetotelluric, inversion, focusing

1. Introduction

[2] The two-dimensional (2-D) magnetotelluric inverse problem has been addressed by several authors. The most well-known approaches are the search for a smooth model [*de Groot-Hedlin and Constable*, 1990; *de Lugao et al.*, 1997; *Mackie et al.*, 1997; *Rodi and Mackie*, 2001] and the rapid relaxation inversion (RRI) [*Smith and Booker*, 1991]. The majority of existing algorithms are based on the minimum norm or maximum smoothness criteria used for stable inversion of magnetotelluric data. The RRI method is also based on approximate calculation of the Frechet derivatives under the assumption that horizontal variations in conductivity are much smaller than vertical ones.

[3] The magnetotelluric (MT) inverse problem, as almost any inverse problem in geophysics, is ill-posed and therefore unstable. It means that one can find several very different geoelectrical models fitting the observed data with the same accuracy. The stable solution of an ill-posed inverse problem can be obtained by using the corresponding regularization methods [*Tikhonov and Arsenin*, 1977]. The regularization is based on a simple idea of searching for a solution within the specific class of selected models. Note that the traditional way to implement regularization in inverse problem solution is based on considering the class of inverse models with smooth distribution of model parameters. Within the framework of the classical Tikhonov regularization, one can select the smooth solution by introducing the corresponding minimum norm, or "smoothing" stabilizing functionals. This approach is widely used in geophysics and has been proved to be a powerful tool for stable inversion of geophysical data. Note that practically all traditional MT inversion methods use the same approach and therefore they produce a smooth image of geoelectrical structures, which in some cases may not describe the geology properly.

[4] It is important to emphasize, however, that regularization does not necessarily mean a smoothing of the solution. The main basis for regularization is the implementation of a priori information

about the geological structure in the inversion procedure. In the case of the traditional smooth inversion this information is provided as an assumption that the solution, the geoelectrical model in the MT case, should be represented by smooth functions. At the same time, in some geological situations it can be useful to consider other assumptions in selecting the class of possible solutions. For example, the traditional smooth inversion algorithms have difficulties in describing the sharp geoelectrical boundaries between different geological formations, while in actual geological situations, sharp boundaries may constitute an important goal of interpretation. This problem arises in inversion for a local conductive target with a sharp boundary embedded in a resistive host rock, which is a typical model in mining exploration. Another example is a marine MT survey to map the salt dome structures in sea bottom geological formations [*Hoversten et al.*, 1998]. Even in general cases of regional geological studies we may be interested in determining large regions with blocky structures. In these situations it can be useful to search for a stable solution within the class of inverse models with blocky geoelectrical structures. The mathematical technique for solving this problem was developed by *Portniaguine and Zhdanov* [1999a]. It is based on introducing a new type of stabilizing functional in inverse problem solution, a so-called minimum support functional. We call this technique a focusing regularized inversion to distinguish it from the traditional smooth regularized inversion.

[5] This technique was successfully applied to the inversion of gravity data [*Last and Kubik*, 1983; *Portniaguine and Zhdanov*, 1999a] to generate a focused and resolved inverse image of the density distribution in a geological cross section. This idea was also implemented in inversion of three-dimensional (3-D) controlled-source MT (CSMT) data over the structures with sharp geoelectrical boundaries [*Portniaguine and Zhdanov*, 1999b; *Zhdanov and Hursan*, 2000]. In this paper we demonstrate that this approach helps to generate much more "focused" and resolved images of blocky geoelectrical structures than conventional MT inversion methods.

[6] We test the focused regularized inversion of magnetotelluric data on synthetic models. We also apply this technique to interpret

the MT data collected in Carrizo Plain, California [Unsworth *et al.*, 1999], and to analyze the MT data collected for mining exploration by INCO Exploration.

2. Principles of Blocky Structure Imaging

[7] The magnetotelluric inverse problem can be formulated as the numerical solution of the following operator equation:

$$A(m) = d, \quad (1)$$

where A is the forward modeling operator, $m = m(r)$ is a scalar function describing geoelectrical model parameter distribution, conductivities $\sigma(r)$ (or resistivities $\rho(r)$), in some volume V in the Earth, ($m \in M$, where M is a Hilbert space of model parameters with an L_2 norm), and d is a geophysical data set ($d \in D$, where D is a Hilbert space of data). Inverse problem (1) is usually ill-posed; that is, the solution can be nonunique and unstable. The conventional way of solving ill-posed inverse problems, according to regularization theory [Tikhonov and Arsenin, 1977; Zhdanov, 1993], is based on minimization of the Tikhonov parametric functional:

$$P^\alpha(m) = \phi(m) + \alpha s(m), \quad (2)$$

where $\phi(m)$ is a misfit functional determined as a square norm of difference between observed and predicted (theoretical) data,

$$\phi(m) = \|Am - d\|_D^2, \quad (3)$$

and $s(m)$ is a stabilizing functional (a stabilizer). The main role of the stabilizer is to select an appropriate class of models for the inverse problem solution. Actually, the stabilizer can be treated as a tool for including a priori information about the geological structures in the inverse problem solution.

[8] There are several common choices for stabilizers, which lead to the different classes of geological models used for inversion. One is based on the least squares criteria or, in other words, on the L_2 norm for functions describing geoelectrical model parameters:

$$s_{L_2}(m) = \|m\|^2 = (m, m) = \int_V m^2 dv = \min, \quad (4)$$

where $(,)$ denotes the inner product multiplication [Parker, 1994]. Another stabilizer uses a minimum norm of difference between the selected model and some a priori model m_{apr} :

$$s_{L_2\text{apr}}(m) = \|m - m_{\text{apr}}\|^2 = \min. \quad (5)$$

The conventional maximum smoothness stabilizing functional uses the minimum norm of the gradient of model parameters ∇m :

$$s_{\text{max sm}}(m) = \|\nabla m\|^2 = (\nabla m, \nabla m) = \min, \quad (6)$$

or, in some cases, the minimum norm of the Laplacian of model parameters $\nabla^2 m$,

$$s_{\text{max sm}}(m) = \|\nabla^2 m\|^2 = (\nabla^2 m, \nabla^2 m) = \min. \quad (7)$$

These functionals have been successfully used in many inversion schemes developed for EM data interpretation [Berdichevsky and Zhdanov, 1984; Constable *et al.*, 1987; Jiracek *et al.*, 1987; Smith and Booker, 1991; Ellis and Oldenburg, 1994; Rodi and Mackie,

2001]. These stabilizers produce smooth geoelectrical models which in some practical situations may not describe properly the real blocky geological structures with sharp boundaries.

[9] Last and Kubik [1983] and Portniaguine and Zhdanov [1999a] considered a different stabilizing functional which minimizes the area of the anomalous model parameters. This functional is called a minimum support (MS) functional, which can be described as follows. Consider the following integral of the model parameter distribution:

$$J_e(m) = \int_V \frac{m^2}{m^2 + e^2} dv, \quad (8)$$

where $e \neq 0$ is a small number, introduced to exclude singularity in the points where $m = 0$.

[10] We introduce the support of m (denoted sptm) or model parameter support, as the combined closed subdomains of V where $m \neq 0$. Then (8) can be modified:

$$J_e(m) = \int_{\text{sptm}} \left[1 - \frac{e^2}{m^2 + e^2} \right] dv = \text{sptm} - e^2 \int_{\text{sptm}} \frac{1}{m^2 + e^2} dv. \quad (9)$$

From (8) we can see that

$$J_e(m) \rightarrow \text{sptm}, \quad e \rightarrow 0. \quad (10)$$

Thus $J_e(m)$ can be treated as a functional, proportional (for a small e) to the model parameter support. We can use the above integral to introduce a minimum support stabilizing functional $s_{MS}(m)$ as

$$\begin{aligned} s_{MS}(m) &= J_e(m - m_{\text{apr}}) = \int_V \frac{(m - m_{\text{apr}})^2}{(m - m_{\text{apr}})^2 + e^2} dv \\ &= \left[\frac{m - m_{\text{apr}}}{[(m - m_{\text{apr}})^2 + e^2]^{1/2}}, \frac{m - m_{\text{apr}}}{[(m - m_{\text{apr}})^2 + e^2]^{1/2}} \right], \end{aligned} \quad (11)$$

where $(,)$, similar to (4), denotes the inner product multiplication.

[11] One can demonstrate that this new functional can be represented in a form similar to the original minimum norm functional. This analogy simplifies the regularized solution of the inverse problem based on the new stabilizer. In order to demonstrate this analogy we introduce a variable weighting function:

$$w_e(m) = \frac{1}{[(m - m_{\text{apr}})^2 + e^2]^{1/2}}, \quad (12)$$

where e is a small number. Then the stabilizing functional (11) can be written as the weighted least squares norm of m :

$$\begin{aligned} s_{MS}(m) &= [w_e(m)(m - m_{\text{apr}}), w_e(m)(m - m_{\text{apr}})] \\ &= (m - m_{\text{apr}}, m - m_{\text{apr}})_{w_e} = \|m - m_{\text{apr}}\|_{w_e}^2, \end{aligned}$$

where the lower subscript “ w_e ” denotes the weighted inner product multiplication and the weighted norm. Using these notations, the corresponding parametric functional can be cast in the form

$$P^\alpha(m) = \|Am - d\|_D^2 + \alpha \|m - m_{\text{apr}}\|_{w_e}^2, \quad (13)$$

which shows that the minimization problem of the parametric functional with the minimum support stabilizer can be treated in a

similar way to the minimization of the conventional Tikhonov functional with the L_2 norm stabilizer $s_{L_2, \text{apr}}(m)$ (equation (5)). The only difference is that now we introduce some a priori variable weighting functions $w_e(m)$ for model parameters. This method is similar to the variable metric method [Press et al., 1987]. However, in our case the variable weighted metric is used in calculation of the stabilizing functional only. The minimization problem for the parametric functional introduced by (13) can be solved using the ideas of traditional gradient type methods [Tarantola, 1987]. In Appendix A we present a description of the reweighted conjugate gradient (RCG) method which we used for MT inversion.

3. Formulation of the Weighted Inverse Solution

[12] In the practical inversion of magnetotelluric data we must remember that we have a finite set of observed data (apparent resistivities and phases at a finite number of observation points for specific frequencies). This set of data forms a matrix \hat{d} in the form of a column of length N .

[13] After discretizing the field data, \hat{d} , and conductivity distribution over the model, $\hat{\sigma} = \hat{m}$, the inverse problem stated in (1) can be written in matrix form:

$$\hat{A}(\hat{m}) = \hat{d}, \quad (14)$$

where \hat{A} is the discrete matrix analogous to the operator A which appears in the numerical solution of the Maxwell's system of equations.

[14] Since the inverse problem (14) is ill-posed, we minimize a parametric functional (13) which is the combination of the misfit and stabilizing functionals [Tikhonov and Arsenin, 1977]. An additional way to constrain the solution is by introducing weights. The data-weighting matrix usually contains information on the importance of one data point with relation to the others. In this way, for example, data of better quality will have a larger weight than data of poor quality. The weights can also be used to normalize data to make them more uniformly distributed. One can also introduce weights for the model parameters to make the sensitivity of the data more uniformly distributed for different model parameters. The parametric functional we seek to minimize is then

$$P^\alpha(\hat{m}_\alpha, \hat{d}) = [\hat{W}_d \hat{A}(\hat{m}) - \hat{W}_d \hat{d}]^* [\hat{W}_d \hat{A}(\hat{m}) - \hat{W}_d \hat{d}] + \alpha (\hat{W}_m \hat{m} - \hat{W}_m \hat{m}_{\text{apr}})^* (\hat{W}_m \hat{m} - \hat{W}_m \hat{m}_{\text{apr}}) = \min, \quad (15)$$

where \hat{W}_d and \hat{W}_m are some weighting matrices of data and model parameters, \hat{m}_{apr} is some a priori model, and the asterisk means transposed matrix. The minimization problem (15) gives us the regularized weighted least squares solution to the inverse problem. Note that practically all existing inversion methods (see, for example, OCCAM MT inversion by de Groot-Hedlin and Constable [1990] or gravity and magnetic inversion by Li and Oldenburg [1998]) use the weighting of the model parameters in one or another form. However, the weights are usually selected on the basis of some simple assumptions about the variation of the sensitivity with the depth to the target. The goal of weighting, usually, is to amplify a weak response and to decrease the strong response in order to resolve the structures located at different distances from the observations. We suggest a new mathematical approach to weighting, based on sensitivity analysis, which automatically makes the sensitivity of the data more uniform to the model parameters.

[15] Let us analyze the sensitivity of the data to the perturbation of one specific parameter m_k . In this case,

$$\delta d_i = F_{ik} \delta m_k, \quad (16)$$

where F_{ik} are the elements of the Frechet derivative matrix computed, for example, using the reciprocity principle [Madden, 1972; Rodi, 1976; McGillvray and Oldenburg, 1990; McGillvray et al., 1994; de Lugao and Wannamaker, 1996; de Lugao et al., 1997]. Following Mehanee et al. [1998], we determine the integrated sensitivity of the data to the parameter m_k as the ratio

$$S_k = \frac{\|\delta d\|}{\delta m_k} = \frac{\sqrt{\sum_i (F_{ik})^2 \delta m_k}}{\delta m_k} = \sqrt{\sum_i (F_{ik})^2}. \quad (17)$$

[16] The diagonal matrix with diagonal elements equal to S_k is called an integrated sensitivity matrix, \hat{S} :

$$\hat{S} = \text{diag}(\hat{F}^* \hat{F})^{1/2}. \quad (18)$$

One can see that the sensitivity depends on the parameter number k . In other words, sensitivity of the data to different parameters is different because the contribution of the different parameters in the observation is also different.

[17] The way of selecting the model parameter weighting matrix can be based on the following consideration. Let us analyze again the stabilizing functional with $\hat{W}_m^2 = \hat{I}$:

$$s(\hat{m}) = (\hat{m} - \hat{m}_{\text{apr}})^* (\hat{m} - \hat{m}_{\text{apr}}). \quad (19)$$

This functional penalizes all departures from the a priori model equally. However, we can weight the model parameters proportionally to the integrated sensitivity of the data to these parameters:

$$s_w(\hat{m}) = (\hat{m} - \hat{m}_{\text{apr}})^* \hat{S} (\hat{m} - \hat{m}_{\text{apr}}). \quad (20)$$

In other words, we can introduce the model parameters weighting matrix as the square roots of the integrated sensitivity matrix:

$$\hat{W}_m = \sqrt{\hat{S}} = \text{diag}(\hat{F}^* \hat{F})^{1/4}. \quad (21)$$

The weighted stabilizer with the weighting matrix $\hat{W}_m = \sqrt{\hat{S}}$ imposes a stronger penalty on the variations from the a priori model for the parameters that contribute to a greater extent to the data. On the contrary, the parameters with a smaller contribution to the data can have a greater range of variations. As a result, in inversion all parameters become practically equally dependent on the data, which leads to a more reliable inverse model solution.

4. Regularized Solution of a Discrete MT Inverse Problem

[18] Now we combine the weighting matrix arising from sensitivity analysis with the variable weighting function of the minimum support stabilizer into one algorithm, minimizing the parametric functional:

$$P^\alpha(\hat{m}) = [\hat{A}(\hat{m}) - \hat{d}]^* [\hat{A}(\hat{m}) - \hat{d}] + \alpha (\hat{m} - \hat{m}_{\text{apr}})^* \hat{w}_e \hat{W}_m^2 (\hat{m} - \hat{m}_{\text{apr}}) = \min, \quad (22)$$

where \hat{W}_m is the constant weighting matrix of model parameters, \hat{m}_{apr} is an a priori model, the asterisk means transposed matrix, and \hat{w}_e is a variable diagonal weighting matrix. Note that in (22) the data-weighting matrix, for simplicity, is set to be equal to the identity matrix. In principle, the data weighting can be easily incorporated in our algorithm. However, the corresponding algebraic equations become too cumbersome. That is why we

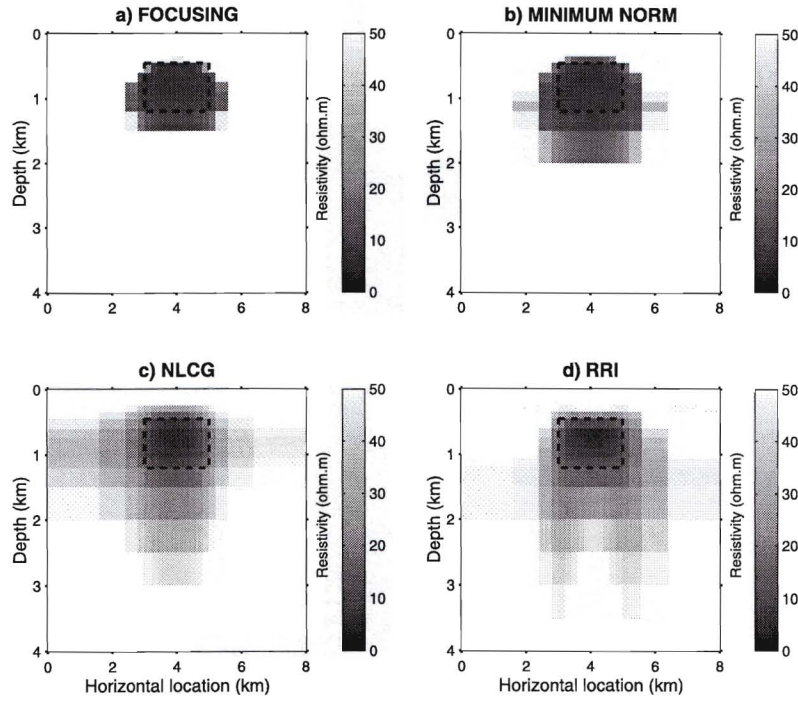


Figure 1. Model 1, 5 ohm m rectangular conductive body (shown by dashed line) embedded in 50 ohm m homogeneous half-space. TE mode inversion results: (a) regularized weighted focusing inversion; (b) regularized weighted minimum norm inversion; (c) NLCG inversion; and (d) RRI inversion.

prefer not to keep matrix \widehat{W}_d^2 in further calculations. Matrix \widehat{W}_m is computed once, using (21),

$$\widehat{W}_m = \sqrt{\widehat{S}} = \text{diag}(\widehat{F}_0^* \widehat{F}_0)^{1/4}, \quad (23)$$

where \widehat{F}_0 is the Frechet derivative matrix of the forward modeling operator, computed for the initial iteration.

[19] Matrix \widehat{w}_e^2 is computed according to (12) so that the diagonal elements of \widehat{w}_e are formed by the values of the function $w_e(m)$ in the corresponding nodes of the model parameter grid:

$$\widehat{w}_e(\widehat{m}) = \text{diag}[(\widehat{m} - \widehat{m}_{\text{apr}})^2 + e^2]^{-1/2}. \quad (24)$$

Substituting (24) and (23) into (22), we arrive at the following formula for the parametric functional P^α :

$$P^\alpha(\widehat{m}) = (\widehat{A}(\widehat{m}) - \widehat{d})^* (\widehat{A}(\widehat{m}) - \widehat{d}) + \alpha (\widehat{m} - \widehat{m}_{\text{apr}})^* \text{diag}[(\widehat{m} - \widehat{m}_{\text{apr}})^2 + e^2]^{-1} \text{diag}(\widehat{F}_0^* \widehat{F}_0)^{1/2} (\widehat{m} - \widehat{m}_{\text{apr}}) = \min. \quad (25)$$

[20] We use the reweighted conjugate gradient method (RCG) in the space of weighted parameters to minimize the parametric functional expressed by (22) or (25). This algorithm is presented in Appendix A. The forward modeling is based on the same numerical implementation of the finite difference method as of *Zhdanov et al.* [1982] and *de Lugao et al.* [1997]. We use the reciprocity principle [Madden, 1972; Rodi, 1976; McGillivray and Oldenburg, 1990; de Lugao and Wannamaker, 1996; de Lugao et al., 1997] for Frechet derivative calculations. Note that according to the construction the minimum support functional generates a stable solution that tends to produce the smallest possible anomalous

domain. It could make the image look unrealistically sharp. Following *Portniaguine and Zhdanov* [1999a], we impose the upper bound $\sigma^+(\mathbf{r})$ and the lower bound $\sigma^-(\mathbf{r})$ for the conductivity values $\sigma(\mathbf{r})$ determined from inversion. During the iterative process we force the model parameter values to fit within these bounds. This algorithm can be described by

$$\begin{aligned} \sigma(\mathbf{r}) &= \sigma^+(\mathbf{r}), & \sigma(\mathbf{r}) &\geq \sigma^+(\mathbf{r}) \\ \sigma(\mathbf{r}) &= \sigma^-(\mathbf{r}), & \sigma(\mathbf{r}) &\leq \sigma^-(\mathbf{r}). \end{aligned} \quad (26)$$

Thus, according to (26) the inverse conductivities $\sigma(\mathbf{r})$ are always distributed within the interval $\sigma^-(\mathbf{r}) \leq \sigma(\mathbf{r}) \leq \sigma^+(\mathbf{r})$. The upper and lower bounds of the conductivity are determined on the basis of a priori information about the physical properties of the rock formations in the inversion area. This information may be available based on the well logging or can be reasonably estimated.

5. Numerical Examples

[21] The 2-D magnetotelluric focusing inversion has been tested on several synthetic models. We present here, as an example, the results obtained for two different models. Model 1 consists of a rectangular conductor with a resistivity of 5 ohm m buried in a 50 ohm m homogeneous half-space. The position of the conductor is shown by the dashed line in Figure 1. Twelve frequencies (0.01, 0.03, 0.1, 0.3, 1, 3, 5, 10, 15, 30, 50, 100 Hz) have been used to generate two sets of synthetic apparent resistivities and phases for transverse electric (TE) and transverse magnetic (TM) modes at 23 stations located at the Earth's surface. The data were contaminated by 4% random noise. The mesh used for the inversion consists of 24 columns and 15 rows, giving rise to 360 blocks to invert for. A 50 ohm m half-space starting model has been used for the TE and TM mode inversions. The a priori model has been selected to be equal to zero ($\widehat{m}_{\text{apr}} = 0$), and the

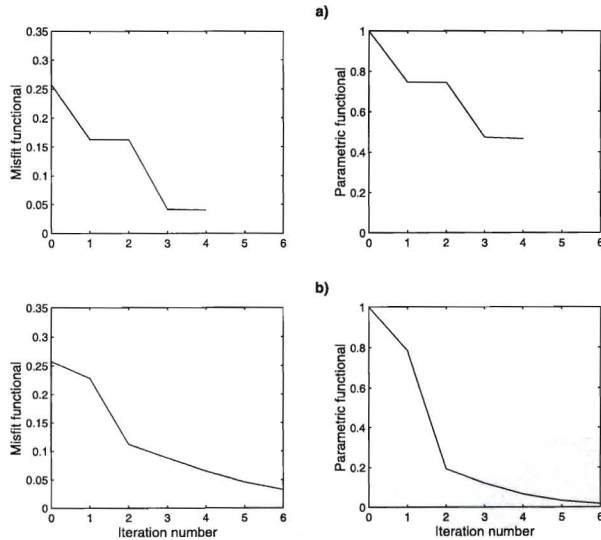


Figure 2. Behavior of the parametric and misfit functionals for the TE mode regularized weighted inversion (top) with focusing and (bottom) with minimum norm.

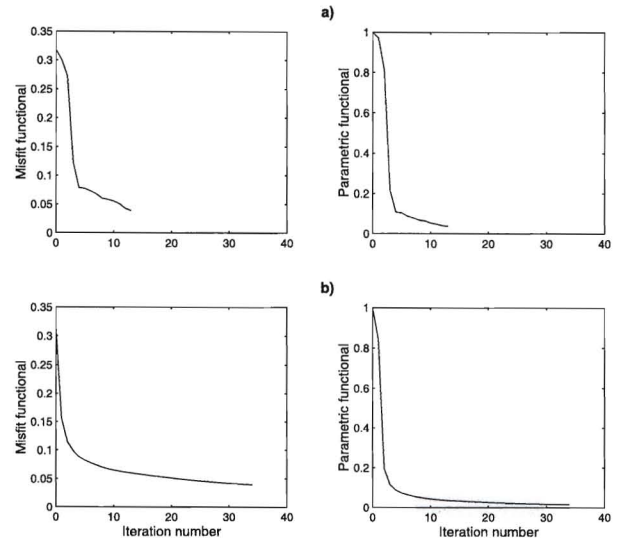


Figure 4. Behavior of the parametric and misfit functionals for the TM mode regularized weighted inversions (a) with focusing and (b) with minimum norm.

upper and lower bounds of focusing inversion resistivities have been set to 50 and 5 ohm m, respectively. The regularization parameter α has been selected automatically on the basis of the algorithm outlined in Appendix A.

[22] Regularized weighted inversion of the TE mode apparent resistivity and phase data without focusing (a minimum norm solution) for a misfit of 4% produces the result shown in Figure 1b. In this case we use only constant weighting matrix \hat{W}_m , assuming $\hat{w}_e = \hat{I}$, where \hat{I} is the identity matrix. The misfit was reached after 6 iterations. Focusing inversion (with variable weighting matrix \hat{w}_e) of the same TE mode data has been performed for a 4% misfit as well and resulted in the model shown in Figure 1a. This misfit was reached after 4 iterations. The

behavior of both the parametric functional normalized by its value computed from the starting model and the misfit functional normalized by the observed data is shown in Figure 2.

[23] The TM mode regularized weighted minimum norm inversion (without focusing) produced a 4% misfit after 34 iterations. The corresponding inversion image is shown in Figure 3b. The TM mode focusing inversion (with the minimum support stabilizer) has been calculated for a misfit of 4% and resulted in the model shown in Figure 3a. The 4% misfit was reached after 13 iterations. The plots of the parametric and misfit functionals are shown in Figure 4. One can see that the focusing inversion converges much faster than the conventional minimum norm inversion. This is because it is more difficult to

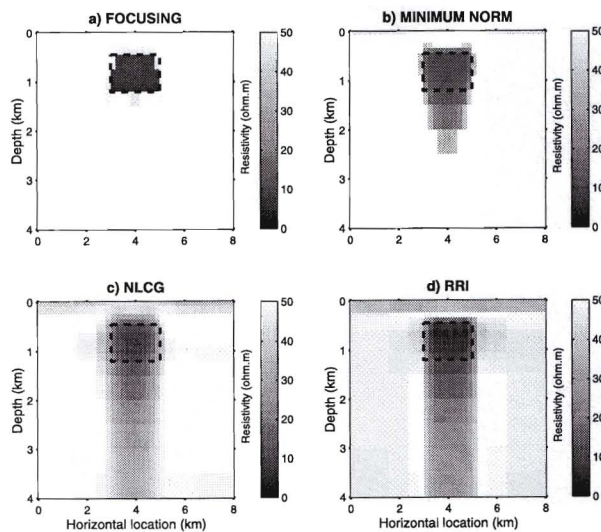


Figure 3. Model 1, 5 ohm m rectangular conductive body (shown by dashed line) embedded in 50 ohm m homogeneous half-space. TM mode inversion results: (a) regularized weighted focusing inversion; (b) regularized weighted minimum norm inversion; (c) NLCG inversion; and (d) RRI inversion.

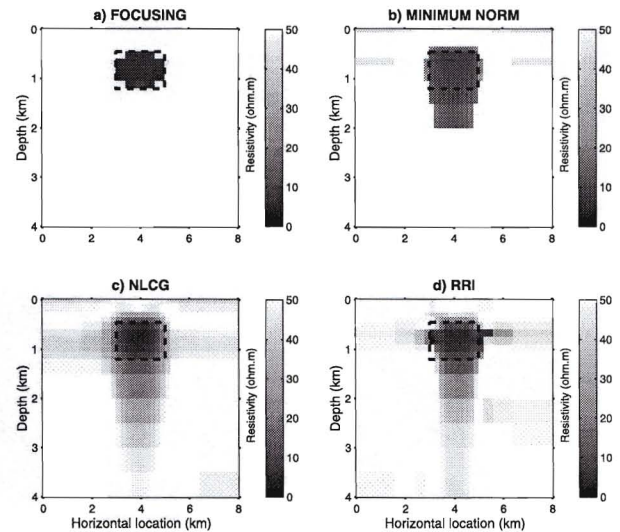


Figure 5. Model 1, 5 ohm m rectangular conductive body (shown by dashed line) embedded in 50 ohm m homogeneous half-space. Joint (TE and TM) inversion results: (a) regularized weighted focusing inversion; (b) regularized weighted minimum norm inversion; (c) NLCG inversion; and (d) RRI inversion.

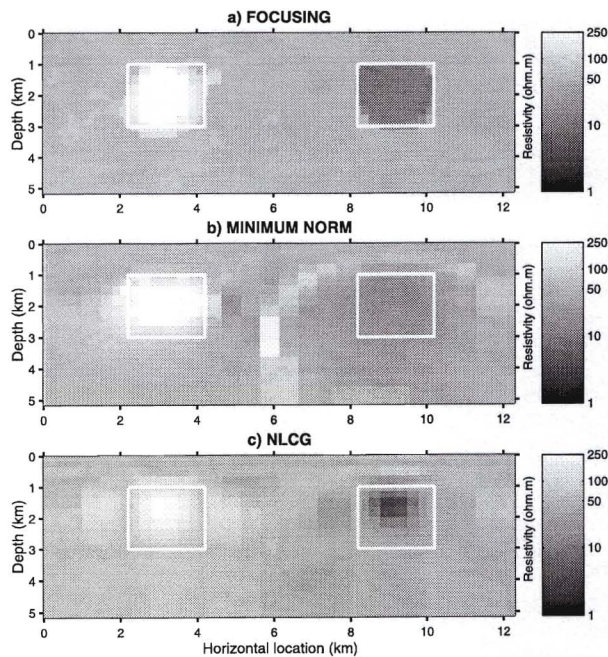


Figure 6. Model 2, 10 and 250 ohm m rectangular bodies (shown by solid white line) embedded in a 50 ohm m homogeneous half-space. Joint (TE and TM) inversion results: (a) regularized weighted focusing inversion; (b) regularized weighted minimum norm inversion; and (c) NLCG inversion.

describe the original blocky structure by the models generated by the code with the minimum norm stabilizer.

[24] For comparison, we inverted the same data using two different codes; the RRI by *Smith and Booker* [1991] and the nonlinear conjugate gradient (NLCG) inversion by *Rodi and Mackie* [2001]. Figures 1c, 1d, 3c, and 3d show the inversion results obtained from these codes for both the TE and TM modes. One can see that RRI and NLCG inversion codes, as one may expect, produce smooth and diffused images which correspond to a traditional smooth stabilizer, incorporated in these codes. Figure 5 shows the inversion results for the joint (TE and TM mode) focusing inversion (Figure 5a), minimum norm inversion (Figure 5b), NLCG (Figure 5c), and RRI (Figure 5d) algorithms, using 50 ohm m homogeneous half-space starting model. One can clearly see that focusing inversion results in a well-resolved image, while all three other techniques produce diffused images.

[25] Model 2 consists of two rectangular bodies with resistivities of 250 and 10 ohm m embedded in a 50 ohm m homogeneous half-space. The locations of these bodies are shown by a bold solid white line in Figure 6. Two sets of synthetic apparent resistivities and phases were generated for TE and TM modes at 51 stations using 14 frequencies (0.01, 0.03, 0.1, 0.3, 1, 3, 5, 10, 15, 30, 50, 100, 300, 1000 Hz). These data were contaminated by 4% random noise. A 50 ohm m half-space starting model has been used for the joint (TE and TM) inversions. The a priori model was set to be equal to zero, and the upper and lower bounds of focusing inversion resistivities were set to 250 and 10 ohm m, respectively. The mesh used for the inversion consists of 52 columns and 26 rows, giving rise to 1352 blocks to invert for. Figure 6 shows the inversion results for the joint (TE and TM mode) focusing inversion (Figure 6a), minimum norm inversion by our code (Figure 6b), and smooth inversion obtained by the NLCG code (Figure 6c). Note that all three models fit the observed data

practically with the same accuracy of 4%. One can clearly see that the focusing joint inversion results in a sharper image. To provide a better comparison between the focusing and smooth images, in Figure 7 we present the horizontal profiles for the resistivity distribution at a depth of 2 km for the inverse models presented in Figure 6. The solid lines in Figure 7 correspond to the true resistivity distribution of the original model at a depth of 2 km. The dashed lines show the inversion results, obtained by focusing inversion (Figure 7a), minimum norm inversion (Figure 7b), and NLCG inversion (Figure 7c). One can clearly see that the minimum norm and NLCG inversions smooth the blocky structure of the original model, especially in the case of conductive body. For comparison, in Figure 8 we present the results of joint (TE and TM) focusing inversion for two different resistivity bounds. Figure 8a shows the joint focusing inversion results corresponding to lower and upper resistivity bounds of 8 and 280 ohm m, respectively. Lower and upper resistivity bounds of 5 and 300 ohm m, respectively, resulted in the joint focusing inversion results shown in Figure 8b. One can see that these images still resolve the two bodies well, especially the conductive one.

[26] Note that we use the blocky model as a true model in our test and therefore arrive at the result that the focusing inversion produces a better image for this model than the smooth inversion. Thus the result of our model study shows that the solution based on the focusing inversion (the blocky structure inversion) is obviously better if we solve the inverse problem for blocky geoelectrical structures. However, if one would solve the inverse problem for the smooth structures, the smooth inversion would generate the better image. We can select one or another class of the inverse models by choosing between different stabilizing functionals in the regularization method. The final decision on which approach is used for a

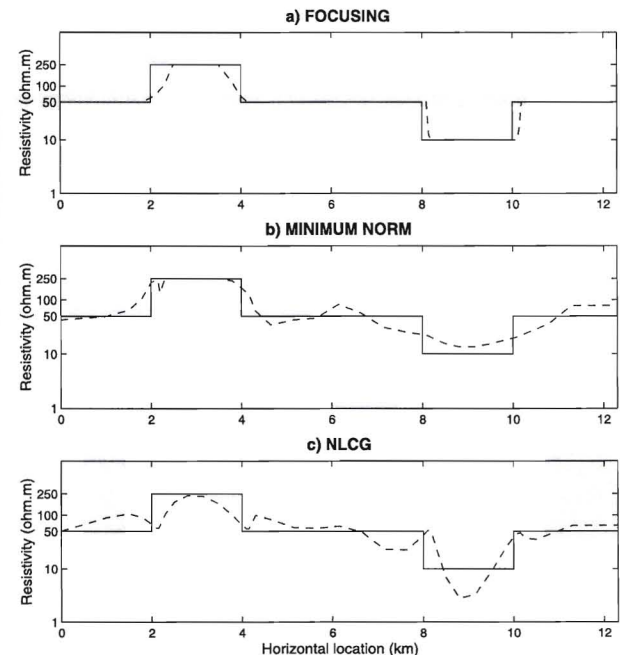


Figure 7. Resistivity distribution from horizontal profile at a depth of 2 km for the joint inversion results of model 2 shown in Figure 6. Solid line presents the true resistivity values. Dashed line presents the resistivity values obtained from inversion: (a) joint regularized weighted focusing inversion; (b) joint regularized weighted minimum norm inversion; and (c) joint NLCG inversion.

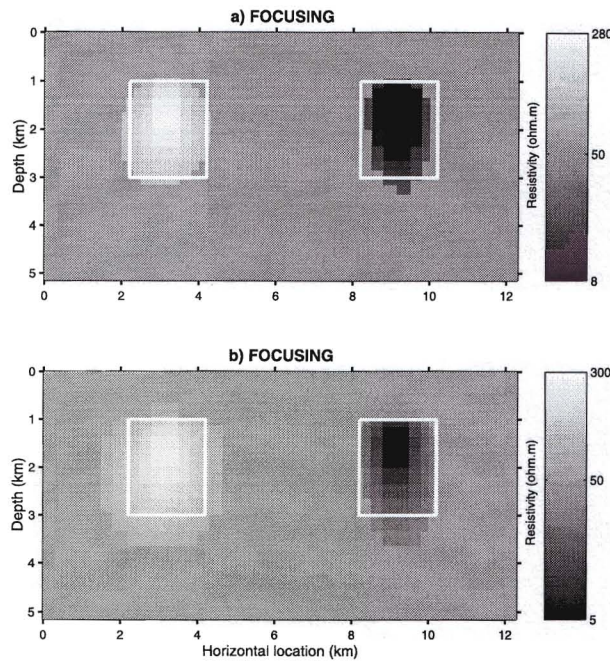


Figure 8. Model 2, 10 and 250 ohm m rectangular bodies (shown by solid white line) embedded in a 50 ohm m homogeneous half-space. Joint focusing inversion results for two different bounds for the inverse resistivity: (a) joint regularized weighted focusing inversion using upper and lower resistivity bounds of 280 and 8 ohm m, respectively; and (b) joint regularized weighted focusing inversion using upper and lower resistivity bounds of 300 and 5 ohm m, respectively.

specific MT data set should be made by the practical geophysicist based on available geological information.

6. Focusing Inversion of MT Data Collected in Carrizo Plain, California

[27] High-resolution magnetotelluric data were collected across the San Andreas Fault (SAF) at Carrizo Plain, California for crustal imaging [Unsworth *et al.*, 1999]. The TE and TM mode regularized weighted inversions with focusing were applied to these data. We expected to find some blocky structures in this area associated with the resistive granitic rock formations. We used a 20 ohm m homogeneous half-space starting model. Figure 9a shows the TM mode regularized weighted inversion results with focusing. The inversion results with focusing for the TE mode data are shown in Figure 10a. One can see that the TE mode inversion shows structures similar to those obtained from the TM mode inversion. The TE and TM joint inversion was performed with focusing using the TM mode inversion results as a starting model. Figure 11a shows the joint focusing inversion results. Figure 11a shows two structures at different depths on the eastern side of the profile. One is a shallow (<1 km depth) conductive occurrence at horizontal locations 5 and 7 km which can be interpreted as a low-resistivity, sandy clay-rich facies of the Monterey shale. The other is a deep resistor centered at ~4 km depth. Note that this resistive structure was also imaged by previous inversions performed for MT data collected across the San Andreas Fault within the Carrizo Plain [Mackie *et al.*, 1997; Unsworth *et al.*, 1999]. At the same time it is commonly accepted that the Great Valley sedimentary units and the Franciscan formation extend westward to the SAF [Page, 1981]. One possible explanation for the resistive structure located east of the SAF is that the resistive body may comprise resistive

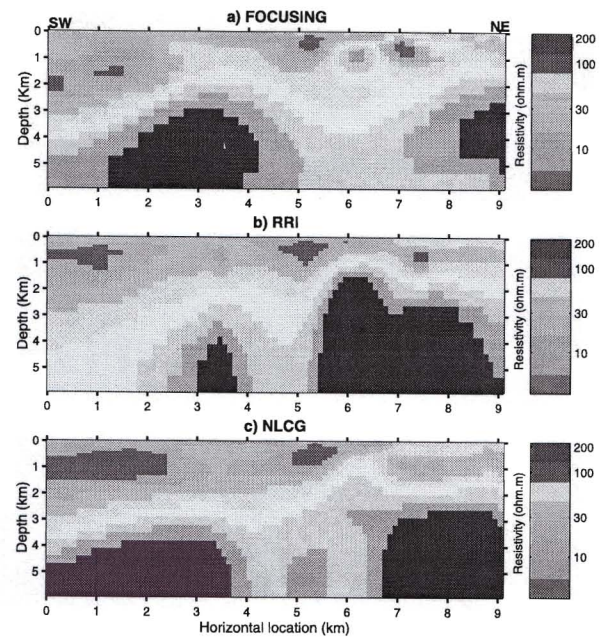


Figure 9. Carrizo Plain, TM inversion results obtained by (a) focusing inversion, (b) RRI, and (c) NLCG.

crystalline rocks. Supporting evidence for the existence of this resistive structure includes the occurrence of granitic rocks in the Crocker Flat-Recruit Pass area near the crest of the Temblors Range, where according to *Simonson* [1962] it appears that crystalline rocks overlie lower Miocene strata. In addition, the Western Gulf Vishnu no. 1 oil well [Graft, 1962] penetrated resistive granitic rocks at 2.11 km depth at a location east of the SAF. Figure 11a shows two other structures on the western side of the profile. The shallow (1–2.5 km depth) conductive structure

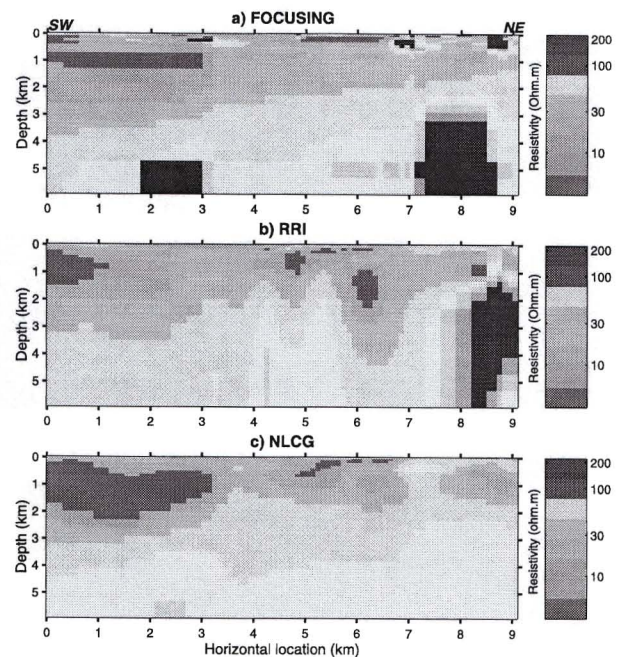


Figure 10. Carrizo Plain, TE inversion results obtained by (a) focusing inversion, (b) RRI, and (c) NLCG.

correlates well with the geologic mapping and well log data for the area under study [Vedder, 1970]. The deep structure is a resistive one located on the western side at a depth >3 km. The transition boundary between the conductive and resistive bodies located on the western side of the profile was identified from seismic reflection performed by Davis *et al.* [1988].

[28] For comparison, Figures 9b, 10b, and 11b show the inversion results obtained by the RRI code, and Figures 9c, 10c, and 11c present the NLCG inversion results. Note that the NLCG, the RRI, and focusing inversion results fit the data equally well, with the same accuracy of 10%, 15%, and 17% for TE, TM, and joint (TE and TM) inversions, respectively. One can see that in general, three different codes, based on the hypotheses of the smooth and blocky conductivity distribution, produce very similar results, probably because the geoelectrical cross section of the Carrizo Plain can be reasonably represented by a smooth model. However, there are some interesting differences. For example, focusing produces more consistent images of conductive and resistive formations for both TE and TM mode data at a depth below 2 km. This contrasts with a striking difference between TE and TM mode inversion results of RRI and NLCG, since the deep resistive structure (located on the western side of the profile) is missing in the TE mode inversion results of RRI and NLCG. Thus this is an example of the practical situation, where we use three different techniques simultaneously to achieve better confidence in the inversion result.

7. Focusing Inversion of MT Data, Collected for Mining Exploration

[29] INCO Exploration conducted an MT survey over an area of known nickel deposits. The goal of this survey was to study the application of the MT method to explore a typical sulphide mineralization zone in complex geological structures. The survey consisted of several lines passing over the prospective mineralization zone. The frequency range of MT data was from 10 to 350 Hz. We selected just one MT line to demonstrate the effectiveness of focusing inversion in this situation. The typical sulphide mineral-

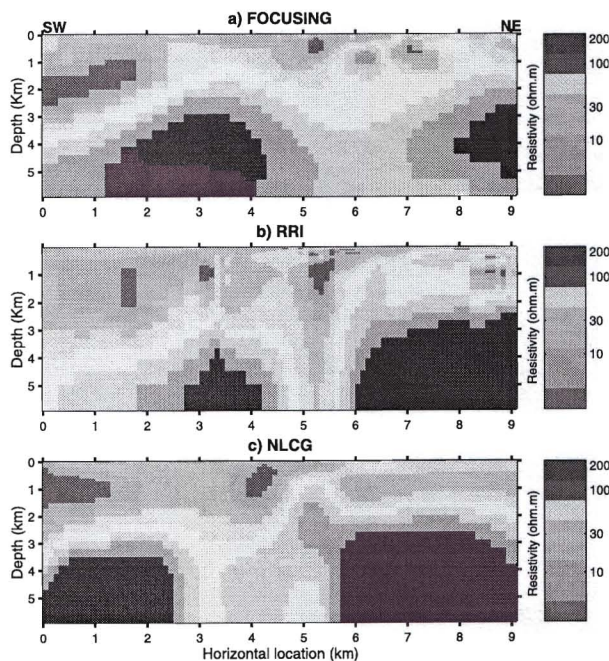


Figure 11. Carrizo Plain, joint (TE and TM) inversion results obtained by (a) focusing inversion, (b) RRI, and (c) NLCG.

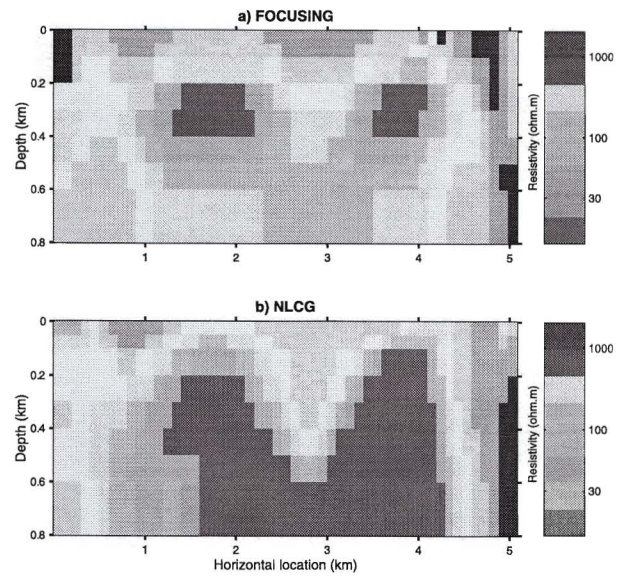


Figure 12. Interpretation of MT data collected for mining exploration, TM inversion results obtained by (a) focusing inversion and (b) NLCG.

ization zone in nickel deposits is composed mainly of pyrrhotite, pentlandite, and chalcopyrite, characterized by a high conductivity. So the geoelectrical targets in this area can be treated as the isolated conductive zones within the host rocks. One can expect that the focusing inversion should resolve this target better than the conventional maximum smoothness approach. Note, also, that the mining target is usually three-dimensional. So 3-D inversion of the array MT data could provide the most reliable information about the mineralization zone. However, in our case we applied the 2-D MT inversion to the profile of TM mode data only in order to get a reasonable first hand evaluation of the mining target. A 1000 ohm m homogeneous half-space was used as a starting model for the focusing and NLCG inversions. Figure 12 shows the results of focusing inversion (Figure 12a) and NLCG inversion (Figure 12b). The misfit for both focusing and NLCG inversion results was 13%. One can see that Figure 12a contains two local conductive targets which can be associated with the known mineralization zones. Figure 12b also shows two conductive anomalies, but they are dispersed and extended at the depth. The focusing inversion, obviously, produces a more compact and clear image of two mineralization zones, which corresponds well to the known geology.

8. Discussion and Conclusion

[30] The main goal of this paper is to demonstrate that there are alternative approaches to MT inverse problem solutions, based on different types of geoelectrical models. The traditional approach uses smooth models to describe the conductivity distribution in rock formations. In this paper, we present a new approach based on approximating the actual geology by the models with the blocky conductivity structures. We can select one or another class of the inverse models by choosing between different stabilizing functionals in the regularization method. The final decision, whose approach should be used for the specific MT data set, should be made on the basis of geological information. If it is known a priori that the geological structure can be reasonably characterized by a smooth model, then the smooth inversion should be used. On the contrary, if it is known a priori that the goal of interpretation is to find blocky structures, like an ore body, conductive fault, or salt

dome structure, then the new method developed in this paper will be more appropriate. In general cases, when there is not enough a priori information about the study area, the best solution would be to try both techniques and to make comparative analysis of two possible geoelectrical cross sections, using both smooth and the focusing inversions. Each of these models will probably fit the data with the same accuracy. The additional geological analysis and the comparison with other geophysical data only could make it possible to select one or another solution. Our code, based on focusing inversion, is designed in such a way that it can generate the minimum norm and the focused solutions simultaneously. This result is reached by a simple selection of the corresponding weighting matrix \hat{w}_e defined by (24). In the case of the minimum norm inversion this matrix is selected to be equal to identity matrix. In the case of the focusing inversion it is a variable matrix, determined by (24). The output of the code consists of two resulting models, fitting the data with the same accuracy but generating two different images. Thus the new technique presented in this paper brings more flexibility in the interpretation of MT data, leaving the final choice of the most suitable model to the user.

[31] We have applied this technique for crustal imaging by inverting the magnetotelluric data acquired in the Carrizo Plain area of California. Our inversion result confirms the principal geoelectrical structures recovered in previous publications [Mackie *et al.*, 1997; Unsworth *et al.*, 1999] but also produces more focused and consistent images of conductive and resistive formations for both TE and TM mode data at depth below 2 km. We suggest that both images, obtained by traditional smooth inversion and by the new method, are useful for further interpretation and analysis because they provide complimentary information about the deep geoelectrical structures. Finally, application of the new focusing inversion to MT data collected for mining exploration by INCO Exploration clearly demonstrates the advantage of the new technique in this situation.

Appendix A: Reweighted Conjugate Gradient (RCG) Method in the Space of Weighted Parameters

[32] The problem of parametric functional minimization (22) can be reformulated in the space of weighted parameters, introduced as

$$\hat{m}^w = \hat{W}_{me} \hat{m}, \quad (A1)$$

where

$$\hat{W}_{me} = \hat{w}_e \hat{W}_m. \quad (A2)$$

We can consider the forward operator which relates the new weighted parameters \hat{m}^w to the data

$$\hat{d} = \hat{A}^w(\hat{m}^w). \quad (A3)$$

In order to keep the same data we should assume

$$\hat{A}^w = \hat{A} \hat{W}_{me}^{-1}. \quad (A4)$$

[33] Using these notations, we can rewrite the parametric functional (22) as

$$P^\alpha(\hat{m}_w, \hat{d}) = [\hat{A}(\hat{W}_{me}^{-1} \hat{m}_w) - \hat{d}] * [\hat{A}(\hat{W}_{me}^{-1} \hat{m}_w) - \hat{d}] + \alpha(\hat{m}^w - \hat{m}_{apr}^w) * (\hat{m}^w - \hat{m}_{apr}^w). \quad (A5)$$

In other words, we keep the same misfit, as in (22), because

$$\begin{aligned} \phi_w(\hat{m}) &= [\hat{A}(\hat{W}_{me}^{-1} \hat{m}_w) - \hat{d}] * [\hat{A}(\hat{W}_{me}^{-1} \hat{m}_w) - \hat{d}] \\ &= [\hat{A}(\hat{m}) - \hat{d}] * [\hat{A}(\hat{m}) - \hat{d}], \end{aligned} \quad (A6)$$

and the same stabilizer, as in (22), equal to the least squares norm of difference $(\hat{m} - \hat{m}_{apr})$ with the weights

$$\begin{aligned} s_w &= (\hat{m}^w - \hat{m}_{apr}^w) * (\hat{m}^w - \hat{m}_{apr}^w) \\ &= (\hat{m} - \hat{m}_{apr}) * \hat{W}_{me}^2 (\hat{m} - \hat{m}_{apr}). \end{aligned} \quad (A7)$$

[34] To construct the iterative process in the space of weighted parameters, one can apply the conventional conjugate gradient method [Tarantola, 1987] to find the minimum of the parametric functional (A5). However, in this case we should take into account the nonlinear character of the transformations (A1) and (A2). Portniaguine and Zhdanov [1999, 1999b] and Zhdanov and Hursan [2000] have developed a more efficient approach to the solution of this problem, based on so-called reweighted regularized conjugate gradient (RCG) method. In the framework of this approach the variable weighting matrix \hat{w}_e is precomputed on each iteration, $\hat{w}_e = \hat{w}_{en} = \hat{w}_e(\hat{m}_n)$ based on the values \hat{m}_n , obtained on the previous iteration. As a result, the weighting matrix \hat{W}_{me} is updated on each iteration as well,

$$\hat{W}_{me} = \hat{w}_{en} \hat{W}_m, \quad (A8)$$

and it is treated as a fixed matrix on each iteration. Therefore the transformations (A1) and (A2) on each iteration can be treated as linear operations, which simplifies significantly all calculations.

[35] This approach uses the idea of adaptive regularization [Zhdanov, 1993], which involves updating the regularization parameter α on each iteration. The only difference is that we update now the regularization parameter and the weighting matrix simultaneously. Note that without adaptive regularization one should solve the minimization problem for parametric functional (A5) many times for different values of the regularization parameter α , which is an extremely time consuming and impractical approach. The adaptive regularization substitutes this complicated procedure by one gradient-type iterative process with the regularization parameter α changing from iteration to iteration. We use similar approach in our reweighted algorithm.

[36] The reweighted RCG method is based on the successive line search in the conjugate gradient direction $\hat{l}(\hat{m}_n)$:

$$\hat{m}_{n+1}^w = \hat{m}_n^w + \delta \hat{m}^w = \hat{m}_n^w - k_n \hat{l}(\hat{m}_n^w).$$

The idea of the line search can be described as follows. We present $P^\alpha[\hat{m}_n^w - k \hat{l}(\hat{m}_n^w)]$ as a function of one variable k and, evaluating it three times along direction $\hat{l}(\hat{m}_n)$, approximately fit it by a parabola and find its minimum and the value of k_n , corresponding to this minimum.

[37] The conjugate gradient directions $\hat{l}(\hat{m}_n^w)$ are selected with the following steps: In the first step we use the gradient direction

$$\hat{l}(\hat{m}_0^w) = \hat{l}(\hat{m}_0^w) = \hat{W}_{me}^{-1} \hat{F} * [\hat{A}(\hat{W}_{me}^{-1} \hat{m}_0^w) - \hat{d}] + \alpha(\hat{m}_0^w - \hat{m}_{apr}^w). \quad (A9)$$

In the next step, the conjugate gradient direction is the linear combination of the gradient in this step and the direction $\hat{l}(\hat{m}_0^w)$ in the

previous step:

$$\tilde{l}(\hat{m}_1^w) = \hat{l}(\hat{m}_1^w) + \beta_1 \tilde{l}(\hat{m}_0^w).$$

In the n th step,

$$\tilde{l}(\hat{m}_{n+1}^w) = \hat{l}(\hat{m}_{n+1}^w) + \beta_{n+1} \tilde{l}(\hat{m}_n^w),$$

where

$$\tilde{l}(\hat{m}_n^w) = \hat{W}_{me}^{-1} \hat{F}^* \left[\hat{A} \left(\hat{W}_{me}^{-1} \hat{m}_n^w \right) - \hat{d} \right] + \alpha \left(\hat{m}_n^w - \hat{m}_{apr}^w \right). \quad (A10)$$

[38] The coefficients β_{n+1} are defined from the condition that the directions $\tilde{l}(\hat{m}_{n+1}^w)$ and $\tilde{l}(\hat{m}_n^w)$ are conjugate:

$$\beta_{n+1} = \frac{\left\| \tilde{l}(\hat{m}_{n+1}^w) \right\|^2}{\left\| \tilde{l}(\hat{m}_n^w) \right\|^2}. \quad (A11)$$

In the last step we recompute the real parameters of the model from the weighted parameters at the n th iteration:

$$\hat{m}_{n+1} = \hat{W}_{me}^{-1} \hat{m}_{n+1}^w = \hat{W}_{me}^{-1} \hat{W}_{en}^{-1} \hat{m}_{n+1}^w. \quad (A12)$$

[39] The regularization parameter α describes the trade-off between the best fitting and most reasonable stabilization. In a case when α is selected to be too small, the minimization of the parametric functional $P^\alpha(\hat{m})$ is equivalent to the minimization of the misfit functional $\phi_w(\hat{m})$; therefore we have no regularization, which can result in an unstable incorrect solution. When α is too large, the minimization of the parametric functional $P^\alpha(\hat{m})$ is equivalent to the minimization of the stabilizing functional $s_w(\hat{m})$, which will force the solution to be closer to the a priori model. Ultimately, we would expect the final model to be exactly like the a priori model, while the observed data are totally ignored in the inversion. Thus the critical question in the regularized solution of the inverse problem is the selection of the optimal regularization parameter α . The basic principles used for determining the regularization parameter α are discussed by *Tikhonov and Arsenin* [1977] and *Zhdanov* [1993]. It can be selected from the progression of numbers

$$\alpha_k = \alpha_0 q^k; \quad k = 0, 1, 2, \dots, n; \quad q > 0. \quad (A13)$$

For any number α_k we can find an element \hat{m}_{α_k} , minimizing $P^{\alpha_k}(\hat{m})$, and calculate the misfit $\left\| \hat{A}(\hat{m}_{\alpha_k}) - \hat{d} \right\|^2$. The optimal value of the parameter α is the number α_{k_0} , for which we have

$$\left\| \hat{A}(\hat{m}_{\alpha_{k_0}}) - \hat{d} \right\|^2 = \delta^2, \quad (A14)$$

where δ is the level of noise in the observed data. The equality (A14) is called the misfit condition.

[40] In our code, as we have mentioned above, we use the adaptive RCG method [Zhdanov, 1993]. In the framework of this method we begin an iteration from a value of α_0 , which can be obtained as a ratio of the misfit functional and stabilizer for an initial model, then reduce α_n according to (A13) on each subsequent iteration and continuously iterate until the misfit condition (A14) is reached.

[41] Note that on each iteration of the reweighted RCG method we actually minimize the parametric functional with the different stabilizers because the regularization parameter and the weighting

matrix W_{en} are updated on each iteration. In order to insure the convergence of the misfit functional to the minimum we check the misfit value on each iteration. We decrease the regularization parameter α if the misfit does not decrease fast enough. This procedure in combination with the parabolic line search in the conjugate gradient direction on every iteration insures the convergence of the method.

[42] **Acknowledgments.** The MT data from the Carrizo Plain were collected with financial support from the USGS under grant 1434-94-6-2423 and from the National Science Foundation under grant EAR 9316160. We are thankful to the University of Washington and, in particular, to Martin Unsworth and Gary Egbert for providing the MT data. We are thankful, also, to INCO Exploration and, in particular, to Alan King and Steve Balch for providing MT data, collected for mining exploration, and permission to publish the inversion results. The authors acknowledge the support of the University of Utah Consortium for Electromagnetic Modeling and Inversion (CEMI), which includes Advanced Power Technologies Inc., AGIP, Baker Atlas Logging Services, BHP Minerals, EXXON-MOBIL Upstream Research Company, INCO Exploration, Japan National Oil Corporation, MINDECO, Naval Research Laboratory, Rio Tinto-Kennecott, 3JTech Corporation, and Zonge Engineering. We are thankful to anonymous reviewers for their useful comments and recommendations, which helped to improve the manuscript.

References

- Berdichevsky, M. N., and M. S. Zhdanov, *Advanced Theory of Deep Geomagnetic Sounding*, 408 pp., Elsevier Sci., New York, 1984.
- Constable, S. C., R. C. Parker, and G. G. Constable, Occam's inversion: A practical algorithm for generating smooth models from EM sounding data, *Geophysics*, 52, 289–300, 1987.
- Davis, T. L., M. B. Lague, W. J. M. Bazeley, S. Gordon, K. McIntosh, and J. S. Namson, Structure of the Cuyama Valley, Caliente Range and Carrizo Plain and its significance to the structural style of the southern Coast Ranges and western Transverse Ranges, in *Tertiary Tectonics and Sedimentation of the Cuyama Basin, San Luis Obispo, Santa Barbara and Ventura Counties, California*, edited by W. J. M. Bazeley, pp. 141–158, Pac. Sect., Soc. of Econ. and Paleontol. Mineral., Bakersfield, Calif., 1988.
- de Groot-Hedlin, C. D., and S. C. Constable, Occam's inversion to generate smooth, two-dimensional models from magnetotelluric data, *Geophysics*, 93, 1613–1624, 1990.
- de Luga, P., and P. E. Wannamaker, Calculating the two-dimensional magnetotelluric Jacobian in finite elements using reciprocity, *Geophys. J. Int.*, 127, 806–810, 1996.
- de Luga, P., O. Portmiguine, and M. S. Zhdanov, Fast and stable two-dimensional inversion of magnetotelluric data, *J. Geomagn. Geoelectr.*, 49, 1469–1497, 1997.
- Ellis, R. G., and D. W. Oldenburg, The pole-pole 3-D DC-resistivity inverse problem: A conjugate gradient approach, *Geophys. J. Int.*, 119, 187–194, 1994.
- Graff, L. B., Exploration drilling in the Carrizo Plain, in *Guidebook to the Geology of Carrizo Plain and San Andreas Fault*, pp. 21–24, San Joaquin Geol. Soc., 1962.
- Hoversten, G. M., H. F. Morrison, and S. C. Constable, Marine magnetotellurics for petroleum exploration, part II, Numerical analysis of subsalt resolution, *Geophysics*, 63, 826–840, 1998.
- Jiracek, G. R., W. L. Rodi, and L. L. Vanyan, Implications of magnetotelluric modeling for the deep crustal environment in the Rio Grande Rift, *Phys. Earth Planet. Inter.*, 45, 179–192, 1987.
- Last, B. J., and K. Kubik, Compact gravity inversion, *Geophysics*, 48, 713–721, 1983.
- Li, Y., and D. W. Oldenburg, 3-D inversion of gravity data, *Geophysics*, 63, 109–119, 1998.
- Mackie, R. L., D. W. Livelybrooks, T. R. Madden, and J. C. Larsen, A magnetotelluric investigation of the San Andreas Fault at Carrizo Plain, California, *Geophys. Res. Lett.*, 24, 1847–1850, 1997.
- Madden, T. R., Transmission system and network analogies to geophysical forward and inverse problems, *Rep. 72-3*, Dep. of Earth and Planet. Sci., Mass. Inst. of Technol., Cambridge, 1972.
- McGillivray, P. R., and D. W. Oldenburg, Methods for calculating Fréchet derivatives and sensitivities for the non-linear inverse problem: A comparative study, *Geophys. Prospect.*, 38, 499–524, 1990.
- McGillivray, P. R., D. W. Oldenburg, R. G. Ellis, and T. M. Habashy, Calculation of sensitivities for the frequency domain electromagnetic problem, *Geophys. J. Int.*, 116, 1–4, 1994.
- Mehanee, S., N. Golubev, and M. S. Zhdanov, Weighted regularized in-

- version of magnetotelluric data, paper presented at International Exposition and Meeting, Soc. of Expl. Geophys., New Orleans, La., 13–18 Sept. 1998.
- Page, B. M., The southern Coast Ranges, in *The Geotectonic Development of California*, edited by W. G. Ernst, pp. 329–416, Prentice-Hall, Old Tappan, N. J., 1981.
- Parker, R. L., *Geophysical Inverse Theory*, 386 pp., Princeton Univ. Press, Princeton, N. J., 1994.
- Portniaguine, O., and M. S. Zhdanov, Focusing geophysical inversion images, *Geophysics*, 64, 874–887, 1999a.
- Portniaguine, O., and M. S. Zhdanov, 3-D focusing inversion of CSMT data, in *Three-Dimensional Electromagnetics, Proceedings of the Second International Symposium*, pp. 132–135, Univ. of Utah, Salt Lake City, 1999b.
- Press, W. H., B. P. Flannery, S. A. Teukolsky, and W. T. Vetterling, *Numerical Recipes: The Art of Scientific Computing*, 818 pp., Cambridge Univ. Press, New York, 1987.
- Rodi, W. L., A technique for improving the accuracy of finite element solutions for magnetotelluric data, *Geophys. J. R. Astron. Soc.*, 44, 483–506, 1976.
- Rodi, W. L., and R. L. Mackie, Nonlinear conjugate gradients algorithm for 2-D magnetotelluric inversion, *Geophysics*, 66, 174–187, 2001.
- Simonson, R. R., Crocker Flat landslide, Recruit Pass area, in *Guidebook to the Geology of Carrizo Plain and San Andreas Fault*, pp. 14–15, San Joaquin Geol. Soc., 1962.
- Smith, J. T., and J. R. Booker, Rapid inversion of two- and three-dimensional magnetotelluric data, *J. Geophys. Res.*, 96, 3905–3922, 1991.
- Tarantola, A., *Inverse Problem Theory*, 613 pp., Elsevier Sci., New York, 1987.
- Tikhonov, A. N., and V. Y. Arsenin, *Solutions of Ill-posed Problems*, 258 pp., John Wiley, New York, 1977.
- Unsworth, M. J., G. D. Egebert, and J. R. Booker, High resolution electromagnetic imaging of the San Andreas Fault in central California, *J. Geophys. Res.*, 104, 1131–1150, 1999.
- Vedder, J. G., Geologic map of the Wells Ranch and Elkhorn Hills quadrangles, San Luis Obispo and Kern Counties, California, *U.S. Geol. Surv. Misc. Geol. Invest. Map*, I-585, 1970.
- Zhdanov, M. S., *Tutorial: Regularization in Inversion Theory*, Colo. Sch. of Mines, Golden, 1993.
- Zhdanov, M. S., and G. Hursan, 3D electromagnetic inversion based on quasi-analytical approximation, *Inverse Problems*, 16, 1–26, 2000.
- Zhdanov, M. S., N. G. Golubev, V. V. Spichak, and I. M. Varentsov, The construction of effective methods for electromagnetic modeling, *Geophys. J. R. Astron. Soc.*, 68, 589–607, 1982.

S. Mehanee and M. Zhdanov, Department of Geology and Geophysics, University of Utah, 135 South 1460 East, RM 719, Salt Lake City, UT 84112-0111, USA. (smehanee@mines.utah.edu; mzhdanov@mines.utah.edu)